Asociación Argentina
de Mecánica Computacional

Mecánica Computacional Vol XXVIII, págs. 2053-2070 (artículo completo)
Cristian García Bauza, Pablo Lotito, Lisandro Parente, Marcelo Vénere (Eds.)
Tandil, Argentina, 3-6 Noviembre 2009

SIMULATION OF 1D AND 2D ELECTROPHORETIC SEPARATIONS IN MICROFLUIDICS CHIPS

Pablo A. Kler[a], Fabio A. Guarnieri[a,b] and Claudio L. A. Berli[c,d]

[a]*CIMEC, INTEC (UNL-CONICET), PTLC, El Pozo, 3000, Santa Fe, Argentina.*

[b]*Fac. de Bioingeniería, UNER, 3100, Oro Verde, Argentina.*

[c]*INTEC (UNL-CONICET), Güemes 3450, 3000, Santa Fe, Argentina*

[d]*Dpto. Físico Matemática, FICH, UNL, Ciudad Universitaria, 3000, Santa Fe, Argentina.*

Keywords: Microfluidic chips, Electrophoresis, Numerical model, PETSC-FEM.

Abstract. Electrophoretic separations comprise a group of analytical techniques such as capillary zone electrophoresis (CZE), isoelectric focusing (IEF), isotachophoresis (ITP) and free flow electrophoresis (FFE). In all cases, separation is based on the dissimilar mobility of ionic species under the action of an external electric field. These techniques, which are widely used in chemical and biochemical analysis, have been miniaturized in the last years and now represent one of the most important applications of the lab-on-a-chip technology. In a previous work, a generalized numerical model of electrophoresis on microfluidic devices was presented. The model is based on the set of equations that governs electrical phenomena (Poisson equation), fluid dynamics (Navier-Stokes equations), mass transport (Nerst-Planck equation) and chemical reactions. Also the relationship between the buffer characteristics (ionic strength, pH) and surface potential of channel walls is taken into consideration. In this work, three application examples are presented: (a) an IEF assay with immobilized pH gradient (IPG) including the influence of electro-osmotic flow on its performance, (b) an IEF assay involving ampholyte-based pH gradient, and (c) a 2D electrophoresis, involving FFIEF plus CZE. The numerical simulation is carried out by using PETSc-FEM (Portable Extensible Toolkit for Scientific Computation - Finite Elements Method), in a Python environment developed at CIMEC using high performance parallel computing and solving techniques based on domain decomposition methods.

1 INTRODUCTION

Electrophoretic separation techniques are based on the mobility of ions under the action of an external electric field (Sommer and Hatch, 2009). These techniques, which are widely used in chemical and biochemical analysis, have been miniaturized in the last years and now represent one of the most important applications of the microscale total analysis systems (μ–TAS) technology (Manz et al., 1990). Electrophoretic separations carried out by μ–TAS technology comprise a group of different techniques such as: capillary zone electrophoresis (CZE), isoelectric focusing (IEF), isotachophoresis (ITP) and free flow electrophoresis (FFE). The benefits of μ–TAS are reduction of consumption of samples and reagents, shorter analysis times, greater sensitivity, portability and disposability (Reyes et al., 2002). Microscopic channels are defined by using materials and fabrication methods that were adopted from the developed microelectronics industry (Koch et al., 2000).

Computational and analytical simulation of on-chip processes serve to reduce the time from concept to chip (Erickson, 2005). However, there are difficulties due to the several orders of magnitude of the relevant length scales involved: the electric double layer (EDL) thickness (in nm), microchannels width (in μm), and microchannels length (in mm). At the same time, the most challenging and interesting aspect of computational simulation of microfluidic chips is the multiphysics nature, which combines fluidics, mass transport, thermal, mechanics, electronics and reaction kinetics. The earliest mathematical model for electrophoresis were developed by Saville and Palusinski (Saville and Palusinski, 1986; Palusinski et al., 1986). This one dimensional models is valid for monovalent analytes in a stagnant electrolyte solution, without electroosmotic flow (EOF). Some of the first numerical simulations of fluid flow and species transport for microfluidic chips were addressed to electrokinetic focusing and sample dispensing techniques (Patankar and Hu, 1998; Ermakov et al., 1998, 2000); they employed an algorithm based on finite volume method in a structured grid. Bianchi et al. (2000) performed 2D finite element simulations artificially increasing the EDL thickness. Arnaud et al. (2002) developed a finite element simulation of isoelectric focusing for ten species, without considering migration nor convection. Chatterjee (2003) developed a 3D finite volume model to study several applications in microfluidics. More recently, Kler et al. (2006, 2007) developed a 3D FEM model to describe the transport of non-charged species by EOF, and Barz and Ehrhard (2005) developed a fully-coupled modeling for electrokinetic flow in microfluidic devices employing 2D finite elements. Different simulations of electrophoretic separations based on IEF techniques were presented by Hruska et al. (2006) and Thormann et al. (2007) in 1D domains, and by Shim et al. (2007) in 2D domains.

In this paper, the generalized numerical model for electrophoretic processes in microfluidic chips previously presented (Kler et al., 2008) is used to simulate three different examples. The model is based on the set of coupled equations that governs flow field, electric field, mass transport and chemical reactions. The relationship between the buffer pH and the electric potential of channel walls is taken into consideration. The numerical simulation is carried out by using high performance parallel computing and solving techniques based on domain decomposition methods (Kler et al., 2009).

2 MODELLING

In this section a brief description of the mathematical model to simulate 3D and time-dependent electrophoretic phenomena in microdevices previously reported (Kler et al., 2008) is presented. The model can also work in 1D and 2D geometric domains, or stationary mode. First

the fluid mechanics and the basis of electroosmotic flow are discussed, then the mass transport balance for all species considered and the chemistry involved are presented.

2.1 Flow field

In the framework of continuum fluid mechanics, fluid velocity u and pressure p are governed by the following set of coupled equations (Probstein, 2003; Li, 2004):

$$-\nabla \cdot \mathbf{u} = 0, \tag{1}$$

$$\rho(\frac{\partial \mathbf{u}}{\partial t} + \mathbf{u} \cdot \nabla \mathbf{u}) = \nabla \cdot \sigma + \rho \mathbf{g} + \rho_e \mathbf{E}, \tag{2}$$

$$\epsilon \nabla \cdot \mathbf{E} = \rho_e \, . \tag{3}$$

Equation (1) expresses the conservation of mass for incompressible fluids. Equation (2) expresses the conservation of momentum for Newtonian fluids of density ρ, viscosity μ, and stress tensor $\sigma = -p\mathbf{I} + \mu(\nabla \mathbf{u} + \nabla \mathbf{u}^T)$, subjected to gravitational field of acceleration $\mathbf{g}$ and electric field intensity $\mathbf{E}$. The last term on the right hand side of Eq.(2) represents the contribution of electrical forces to the momentum balance, where $\rho_e = F \sum_k z_k c_k$ is the electric charge density of the electrolyte solution, obtained as the summation over all type-k ions, with valence z_k and molar concentration c_k, and F is the Faraday constant.

Equation (3) (Poisson equation) establishes the relation between electric field and charge distributions in the fluid of permittivity ϵ. Here it is relevant to mention that the ion distributions c_k (to be included in Eqs. (2) and (3) through ρ_e must be derived from Nernst-Planck equation, which accounts for the flux of type-k ions due to electrical forces, fluid convection and Brownian diffusion (Probstein, 2003). This coupling can be avoided by introducing the following approximation.

2.2 Thin EDL approximation

The thickness of the EDL is quantified through Debye length (Probstein, 2003; Hunter, 2001). For the ionic concentrations normally used in practice, this thickness is in the order of $1 - 10\ nm$, while cross-sectional channel dimensions are in the $10 - 100\ \mu m$ range. Consequently, in most of the flow domain $\rho_e \approx 0$, except in the close vicinity of charged interfaces. When an external electric field $\underline{\nabla}\phi_a$ is applied tangent to the interface, the electric forces acting on excess ions in the EDL drag the surrounding liquid, and thus EOF develops. For thin EDL in relation to the channel width, the effect is confined to a certain plane parallel to the channel wall, also designated shear plane, where the surface potential is the electrokinetic potential (ζ). Under these conditions, the electro-osmotically driven flow can be regarded as the result of an electrically-induced slip velocity, the magnitude of which is:

$$\mathbf{u}_{EO} = -\frac{\epsilon \zeta}{\mu} \nabla \phi_a \tag{4}$$

Due to the fact that $\rho_e \approx 0$, $\nabla \phi_a$ can be calculated from Laplace's equation:

$$\nabla^2 \phi_a = 0 \tag{5}$$

Further, the last term on the RHS of Eq. (2) vanishes, and the EOF is considered by using Eq. (4) as a boundary value at channel walls.

2.3 Electric potential

Equation (5) is the simplest way to obtain the electric potential field in the flow domain. Nevertheless, this equation does not take into account possible variations of the electric field due to ion distributions. In order to consider (local) non-zero charge density due to buffer constituents or sample concentrations in the fluid, Eq. (6) is introduced,

$$\nabla \cdot \mathbf{i} = 0 \tag{6}$$

where $\mathbf{i}$ is the electric current density. Specifically, the current density is given by the sum of different fluxes of charged species:

$$\mathbf{i} = F \sum_{j=1}^{N} z_j \mathbf{j}_j \tag{7}$$

where $\mathbf{j}_j$ is the molar flux of the j-specie, established by the Nerst-Plank equation:

$$\mathbf{j}_j = -\Omega_j z_j F c_j \nabla \phi - D_j \nabla c_j + c_j \mathbf{u}. \tag{8}$$

In Eq. (8), Ω_j and D_j are the ion mobility and diffusivity, respectively. Finally by combining Eqs. (6), (7) and (8), Eq. (9) is obtained:

$$\nabla \cdot (-F^2 \sum_{j=1}^{N} z_j^2 \Omega_j c_j \nabla \phi - F \sum_{j=1}^{N} z_j D_j \nabla c_j + F \sum_{j=1}^{N} \mathbf{u} z_j c_j) = 0 \tag{9}$$

which enables to solve the electric potential. It should be noted here that ϕ is the total potential, which is regarded as the superposition of the applied potential ϕ_a and the one generated by local variations in conductivity.

2.4 Mass transport and chemistry

The mass transport of weakly concentrated sample ions and buffer electrolyte constituents can be modeled by a linear superposition of migrative, convective and diffusive transport mechanisms and a reactive term. In a non-stationary mode, for the j-type species, this is:

$$\frac{\partial c_j}{\partial t} + \nabla \cdot (-z_j \Omega_j \nabla \phi c_j + \mathbf{u} c_j - D_j \nabla c_j) - r_j = 0 \tag{10}$$

Different components, weak electrolyte analytes and buffer components (acids, bases and ampholytes), strong analytes, and the hydrogen ion particularly have to be considered. In electrolyte chemistry the processes of association and dissociation are much faster than the transport electrokinetic processes, hence, it appears to be a good approximation to adopt chemical equilibrium constants to model the reactions present in our problem. In this sense, the strong electrolytes are considered as completely dissociated. The expressions of r_j were presented previously (Kler et al., 2008).

2.5 Electrokinetic potential as a function of the electrolyte composition

The electrokinetic potential at the solid-fluid interface depends on the charge generation mechanism of the surface. In principle, it may be thought that solid walls expose toward the fluid a certain number of specific sites (n_S) able to release or take H^+ ions, with a dissociation constant K_S. In equilibrium with an aqueous electrolyte solution, the surface becomes electrically charged. For the case of interfaces containing weak acid groups, such as silanol in fused silica capillaries and carboxyl in synthetic polymer materials, the following relationship is appropriate (Berli et al., 2003):

$$(8\epsilon k_B T c^{(b)})^{(\frac{1}{2})} \sinh(\frac{ze\zeta}{2k_B T}) = \frac{-en_s}{1+10^{(pK_S-pH)}e^{-e\zeta/k_B T}} \tag{11}$$

Therefore, if the parameters that characterize the interface are known (n_S, K_S), the ζ-potential can be readily predicted for different values of pH and bulk ion concentrations $c^{(b)}$. Then the electro-osmotic velocity is directly coupled to the electrolyte composition. Empirical formulae were also reported in order to simplify calculations (Kirby, 2004).

3 SIMULATION TOOLS

3.1 Software

All numerical simulations presented were performed within a Python programming environment built upon *MPI for Python* (Dalcín et al., 2008), *PETSc for Python* (Dalcín, 2005-2008), and *PETSc-FEM* (Sonzogni et al., 2002). PETSc-FEM is a parallel multiphysics code primarily targeted to 2D and 3D finite elements computations on general unstructured grids. PETSc-FEM is based on MPI and PETSc (Balay et al., 2008), it is being developed since 1999 at the *International Center for Numerical Methods in Engineering* (CIMEC), Argentina. PETSc-FEM provides a core library in charge of managing parallel data distribution and assembly of residual vectors and Jacobian matrices, as well as facilities for general tensor algebra computations at the level of problem-specific finite element routines. Additionally, PETSc-FEM provides a suite of specialized application programs built on top of the core library but targeted to a variety of problems (e.g., compressible/incompressible Navier–Stokes and compressible Euler equations, general advective-diffusive systems, weak/strong fluid-structure interaction). In particular mass transport, chemistry and fluid flow computations presented in this article are carried out within the Navier–Stokes module available in *PETSc-FEM*. This module provides the required capabilities for simulating mass transport and incompressible fluid flow through a monolithic *SUPG/PSPG* (Tezduyar et al., 1992; Tezduyar and Osawa, 2000) stabilized formulation for linear finite elements. Electric Computations are carried out with the Laplace's and the Charge Conservation modules.

3.2 Hardware

Simulations were carried out using a Beowulf cluster *Aquiles* (Storti, 2005-2008). The hardware consists of 82 disk-less single processor computing nodes with Intel Pentium 4 Prescott 3.0GHz 2MB cache processors, Intel Desktop Board D915PGN motherboards, Kingston Value RAM 2GB DDR2 400MHz memory, and 3Com 2000ct Gigabit LAN network cards, interconnected with a 3Com SuperStack 3 Switch 3870 48-ports Gigabit Ethernet.

4 NUMERICAL EXAMPLES

In what follows, three different numerical examples are presented. First a classical example from the literature (Palusinski et al., 1986) of IEF by immobilized pH gradient (IPG),including effects of EOF. Second, a simulation of IEF by ampholyte-based pH gradient, and finally a simulation of 2D electrophoretic process in a 3D geometry is presented: FFIEF (free flow isoelectric focusing)+ CZE.

4.1 Histidine IEF by IPG

4.1.1 Stagnant fluid

Simulation of IEF in a straight channel (1 cm x 1 mm) is presented here. First we compare results with those in the literature (Palusinski et al., 1986; Chatterjee, 2003; Shim et al., 2007), which involve no bulk flow. The aminoacid Histidine is focused in the channel. IPG is achieved by immobilizing buffer constituents cacodylic acid (CACO) and tris(hydroxymethyl)-aminoetane (TRIS). Physicochemical properties of analyte and buffer constituents considered in this problem are summarized in Table 1.

Concentration of buffer constituents are determined in a suitable way to obtain pH profile along the center of the channel, as is shown in Figure 1.

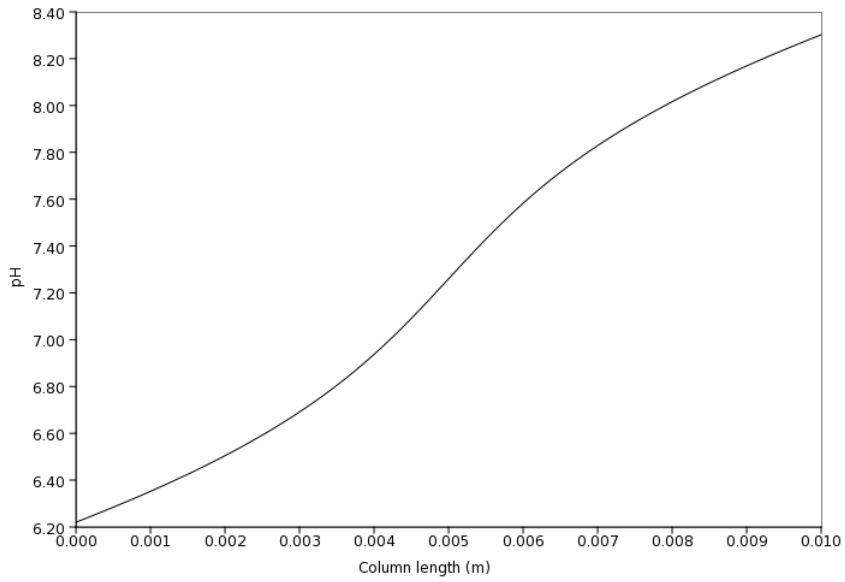

Figure 1: pH profile along the center of the channel.

After IPG is determined, a sample of 1 mM Histidine is injected in the whole channel. Then potential is applied in such a way that a constant density current of $0.2Am^{-2}$ is generated along the channel. The anode is at the left and cathode at the right of the channel. Concentration of focused histidine and conductivity profiles at different time at the center of the channel are showed in Figure 2 and 3 respectively. Figure 4 shows 2D profiles for histidine concentration at different times.

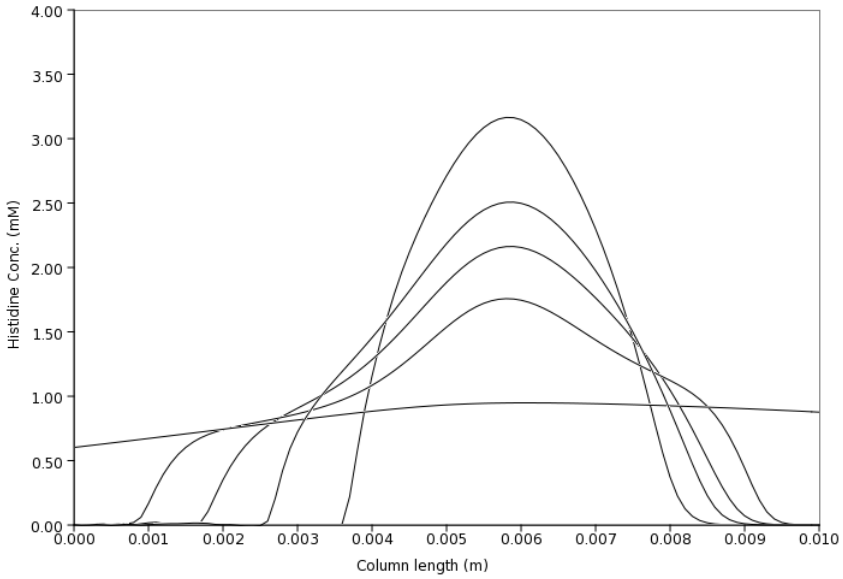

Figure 2: Concentration profiles of histidine at 0, 10, 20, 30 and 40 minutes.

Analyte	**Dissociation constants**	**Mobility** ($m^2V^{-1}s^{-1}$)	**Diffusivity** (m^2s^{-1})
Histidine	$pK1 = 6.04; pK2 = 9.17$	$2.02\ 10^{-8}$	$5.22\ 10^{-10}$
CACO	$pK1 = 6.21$	0.0	0.0
TRIS	$pK1 = 8.30$	0.0	0.0

Table 1: Physicochemical properties of analyte and buffer constituents.

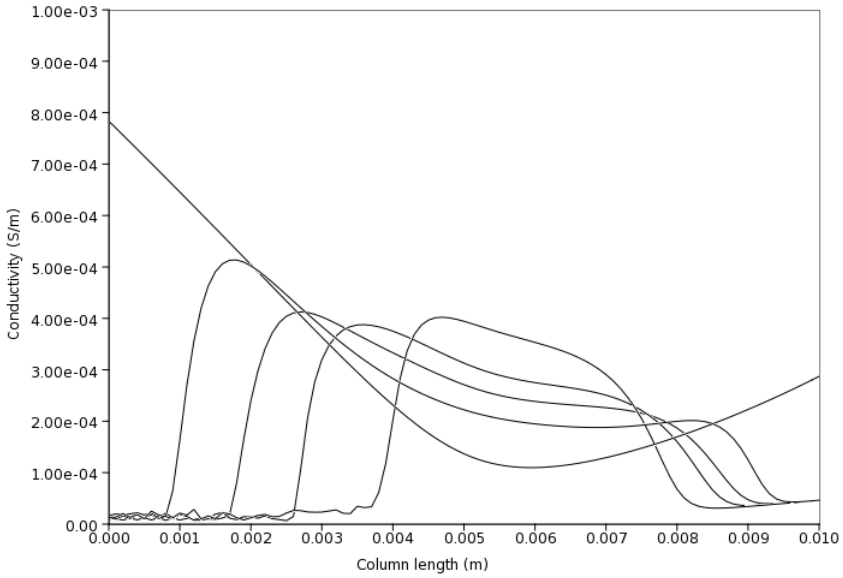

Figure 3: Conductivity profiles at 0, 10, 20, 30 and 40 minutes.

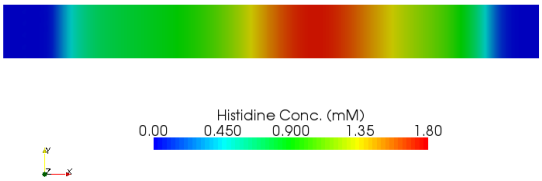

(a) 10 minutes.

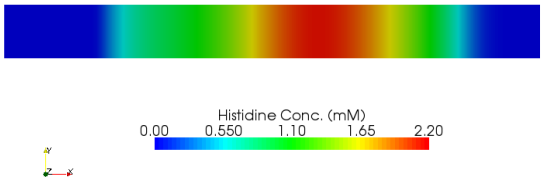

(b) 20 minutes.

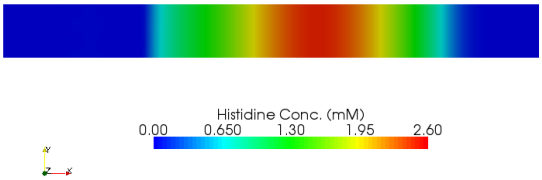

(c) 30 minutes.

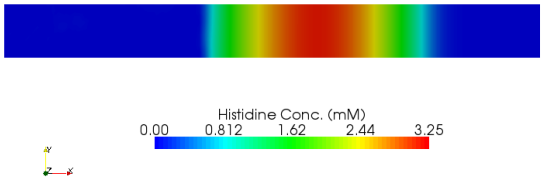

(d) 40 minutes.

Figure 4: Histidine concentration profiles at 10, 20, 30 and 40 minutes.

4.1.2 EOF effects

Previous results were obtained by supposing no bulk flow. In practice this situation is not fully reachable because the ζ-potential cannot be reduced to zero, which has strong effects in focusing performance. Next calculations describe the previous problem with bulk flow due to the presence of EOF. The magnitude of the flow is related to the applied electric field, the wall electric properties and buffer solution composition as was described in section 2.5. In this case, applied electric field and buffer composition are the same as in the previous case.

Equation (11) was used in order to calculate ζ-potential. We considered $pK_s = 7.0$ and $n_s = 1.22\ 10^{16} + 7.3\ 10^{16} c_0$ in our calculations, where c_0 is the bulk ion concentration near the considered wall portion. The relation between pH and ζ-potential is shown in Figure 5.

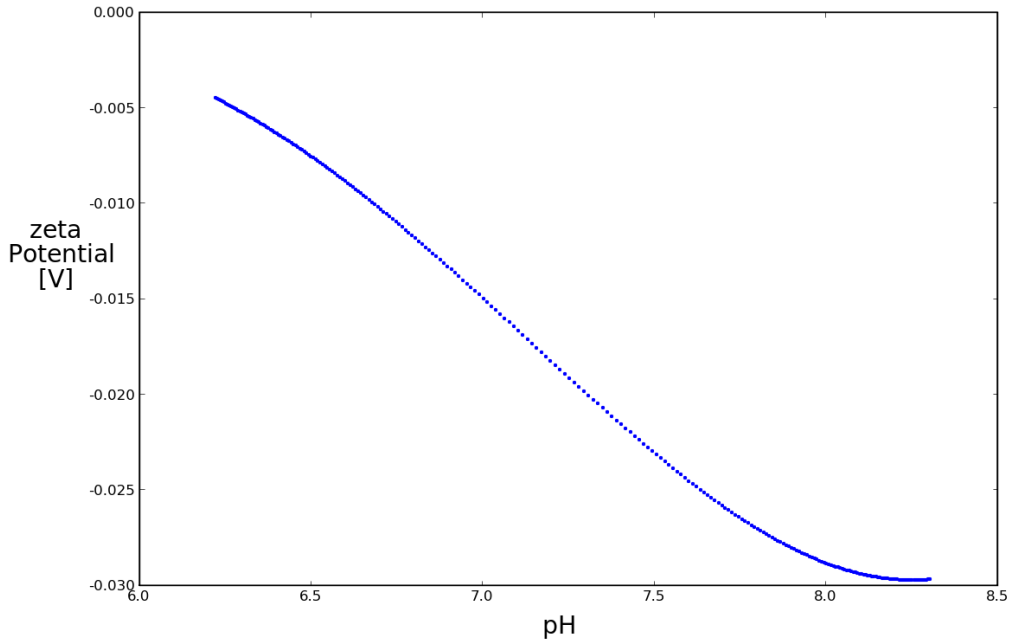

Figure 5: ζ-potential as a function of buffer pH.

Figure 6 shows electric field, pressure and velocity distributions. A strong coupling between them can be easily inferred. Figure 7 shows Histidine concentration profiles at different times. Focusing efficiency decreases due to the sample dispersion (non uniform velocity profile) and due to the reduction of the residence time of the species in the channel.

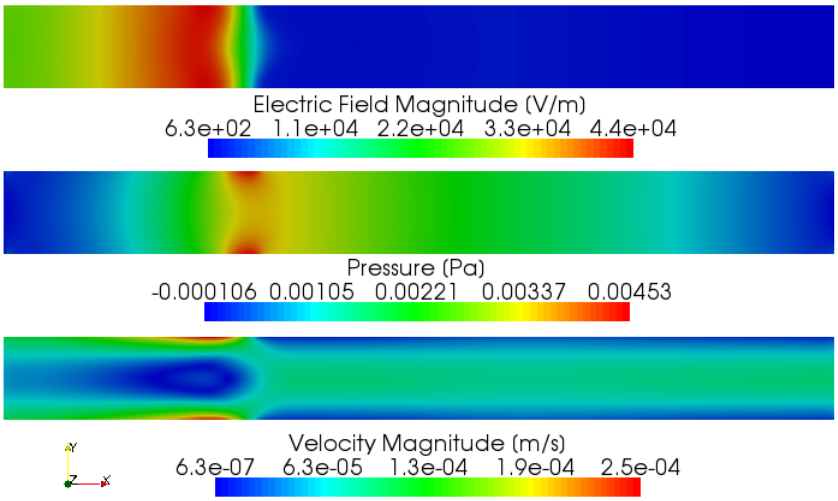

Figure 6: Electric field, pressure and velocity distributions after 2 minutes.

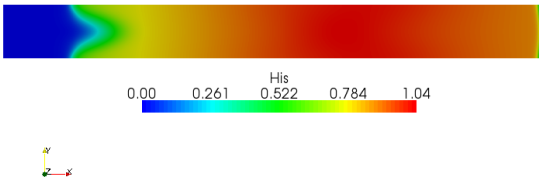

(a) 1 minute.

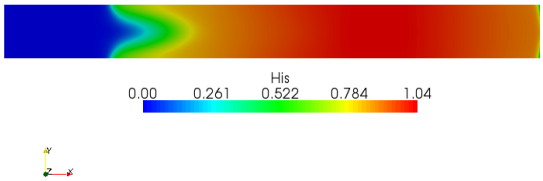

(b) 1.5 minutes.

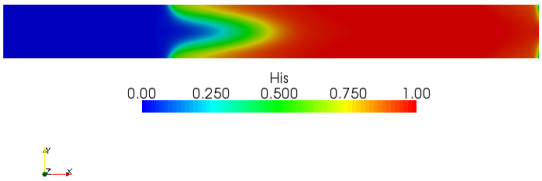

(c) 2 minutes.

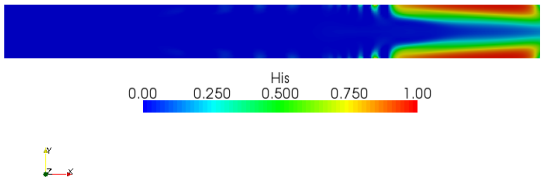

(d) 2.5 minutes.

Figure 7: Histidine concentration profiles at 1, 1.5, 2 and 2.5 minutes.

4.2 IEF by ampholyte-based pH gradient

In this example another IEF process is simulated. In this case pH gradient is generated by ampholytes in solution that, under the effect of an electric field are focused around its isoelectric point, and determine different pH steps in the channel. Ten ampholytes and one protein. Physicochemical properties are summarized in Table 2. Potentials applied are $0V$ for the cathode and $100V$ for the anode. Initially ampholytes and protein are uniformly distributed in the channel, and ampholyte concentration is ten times larger than protein concentration.

Figures 8 and 9 show ampholyte and protein concentration at different times. Figure 10 shows pH gradient evolution with time. Finally Figures 11a and 11b shows concentration distribution in the 2D domain for pH and protein respectively.

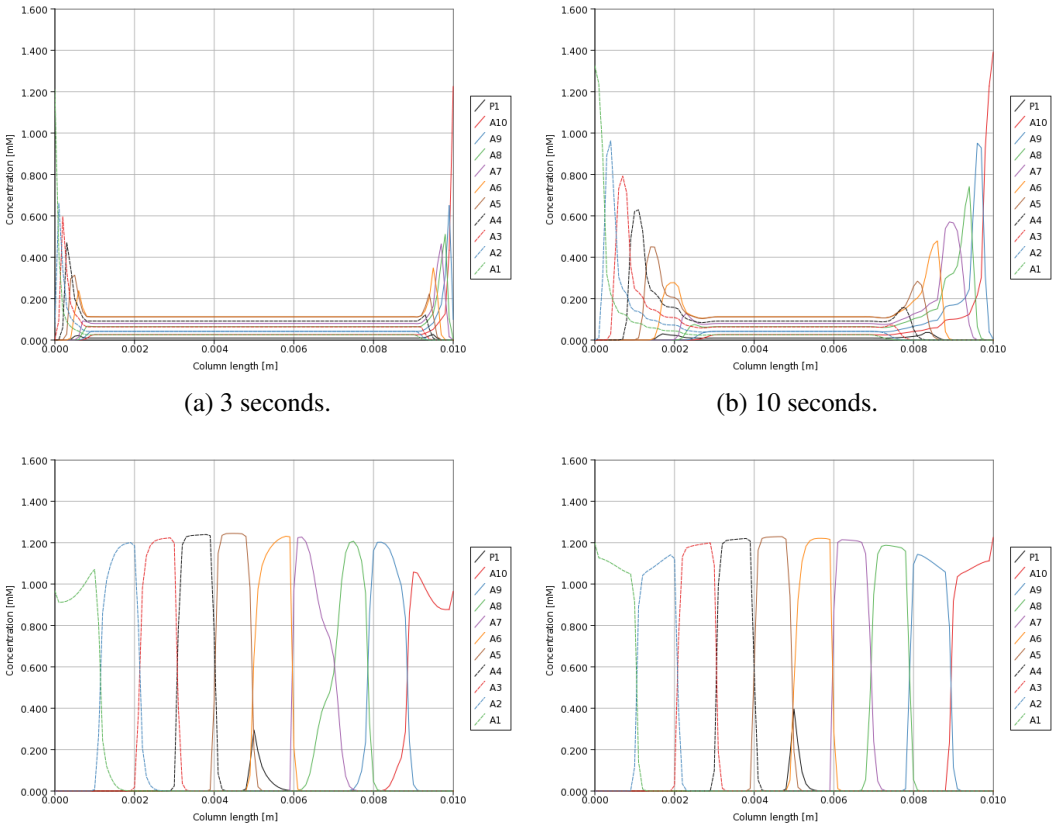

(a) 3 seconds.

(b) 10 seconds.

(c) 40 seconds.

(d) 80 seconds.

Figure 8: Ampholyte and protein concentration along the center of the channel at 3, 10, 40 and 80 seconds.

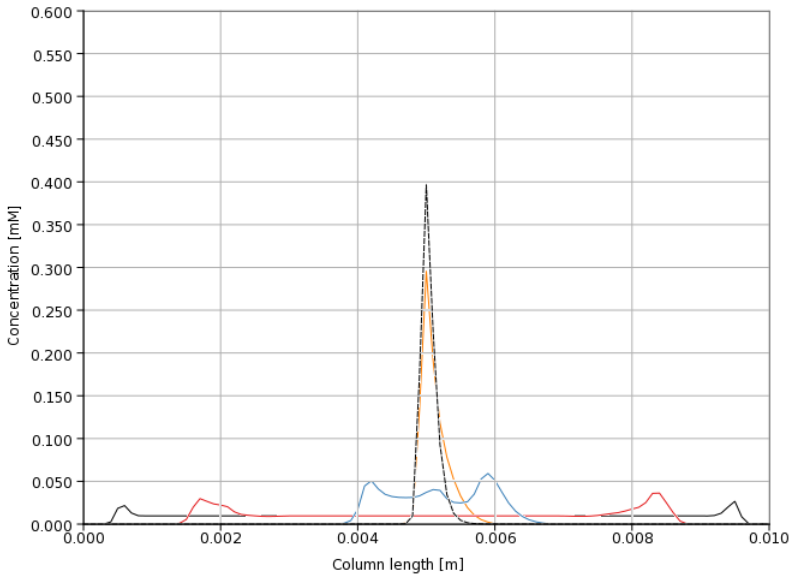

Figure 9: Protein distribution along the center of the channel for 3, 10, 25, 40 and 80 seconds.

Component	pK_1	pK_2	pI	**Mobility** ($m^2V^{-1}s^{-1}$)
Ampholyte 1	6.01	6.41	6.21	$3.0\ 10^{-8}$
Ampholyte 2	6.25	6.65	6.45	$3.0\ 10^{-8}$
Ampholyte 3	6.47	6.87	6.67	$3.0\ 10^{-8}$
Ampholyte 4	6.71	7.11	6.91	$3.0\ 10^{-8}$
Ampholyte 5	6.94	7.34	7.14	$3.0\ 10^{-8}$
Ampholyte 6	7.17	7.57	7.37	$3.0\ 10^{-8}$
Ampholyte 7	7.51	7.91	7.71	$3.0\ 10^{-8}$
Ampholyte 8	7.64	8.04	7.84	$3.0\ 10^{-8}$
Ampholyte 9	7.87	8.50	8.30	$3.0\ 10^{-8}$
Ampholyte 10	8.10	8.50	8.30	$3.0\ 10^{-8}$
Protein	7.00	7.60	7.30	$3.0\ 10^{-8}$

Table 2: Physicochemical properties of buffer and analyte constituents.

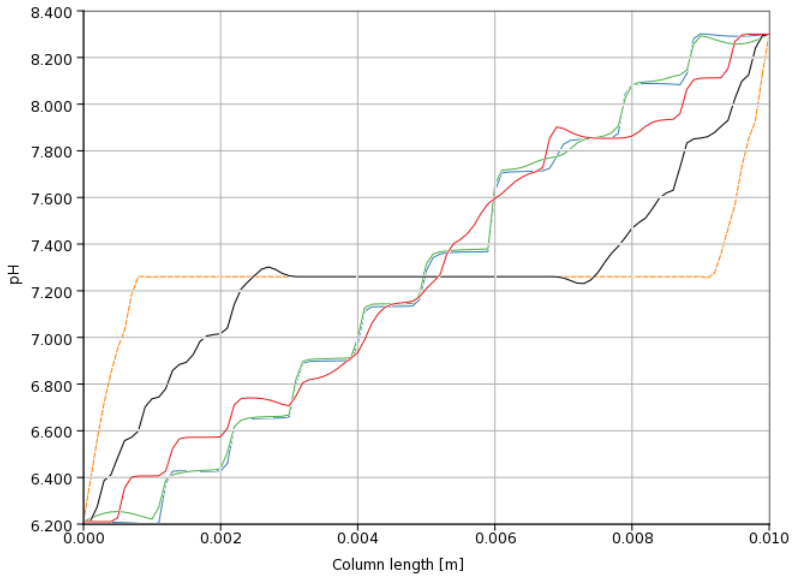

Figure 10: pH distribution along the center of the channel for 3, 10, 25, 40 and 80 seconds.

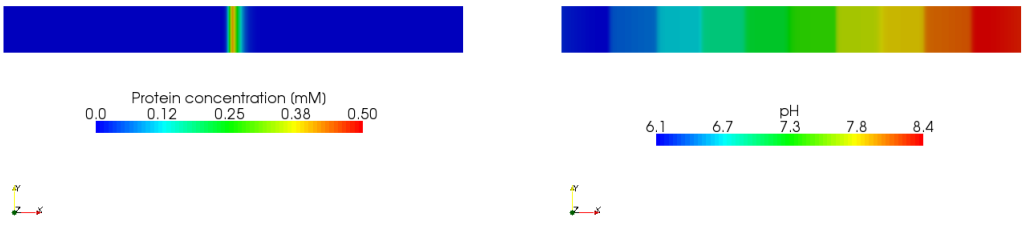

(a) Protein concentration. (b) pH.

Figure 11: Protein and pH distributions in the channel after 80 seconds. Vertical axis is scaled by 10 in order to achieve a correct visualization.

4.3 2D Electrophoresis: FFIEF + CZE

This example shows a practical problem (Kohlheyer et al., 2006) coupling a recent technique, as FFIEF, and a classical one, CZE. This problem represents a challenge for the computational model due to its tridimensional characteristics, the complex chemistry involved, and the strong coupling between the electric field, velocity field, and concentration fields. The geometry for the problem consists in a microfluidic network, with trapezoidal section, with a primary section in which FFIEF is carried out (the reactor), and a second one with three channels for the CZE process(secondary channels). The walls of the reactor have a fixed pH (6.2 and 8.3) and potentials are applied at these walls in order to perform the FFIEF. Additionally, at the exits of the secondary channels, potentials are applied in order to generate EOF and the second electrophoretic separation (CZE). Figure 12 shows the geometry and the electric potential for the problem.

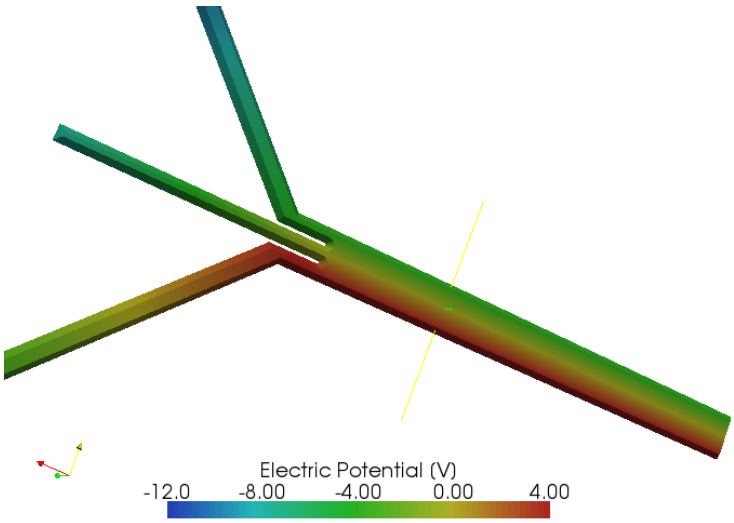

Figure 12: Geometry and electric potential distribution for the 2D electrophoresis problem.

In order to generate an appropriate pH gradient for the FFIEF, ten ampholytes are considered in solution with a concentration of $0.1\ mM$ each. Properties of ampholytes are listed in Table 2. The aim of the process is to achieve a bidimensional electrophoretic separation of sample matrix of 6 different proteins. Physicochemical properties of these proteins are listed in Table 3.

Proteins are injected after the pH gradient takes the stationary form. This distribution, and the streamlines for the velocity field (also stationary) are shown in Figure 13.

Depending on isoelectric points, proteins focus at different pH regions and move along different streamlines. Following these streamlines, when proteins leave the reactor, they get into different secondary channels, depending on its pI. Figure 14 shows total sample concentrations at different times. In this figure the process of separation across the reactor is shown. Figure 15 shows results for the CZE process at central secondary channel.

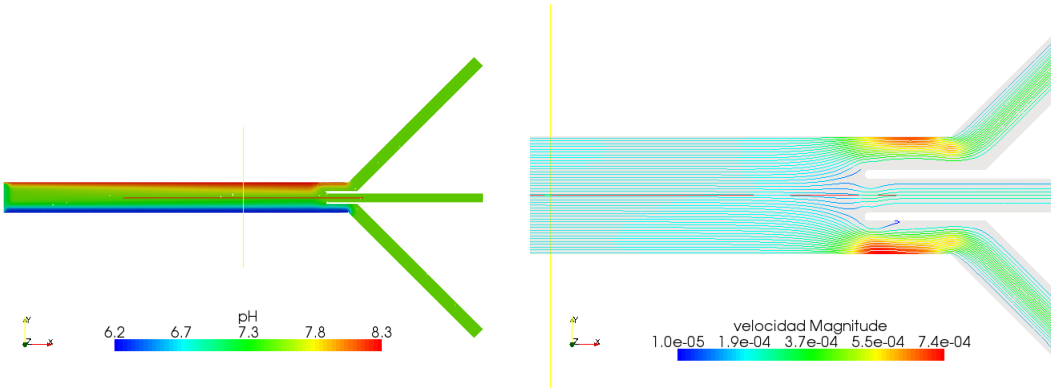

(a) pH distribution. (b) Streamlines for the velocity field.

Figure 13: pH distribution and streamlines for the velocity field in a slice plane at $z = 0$.

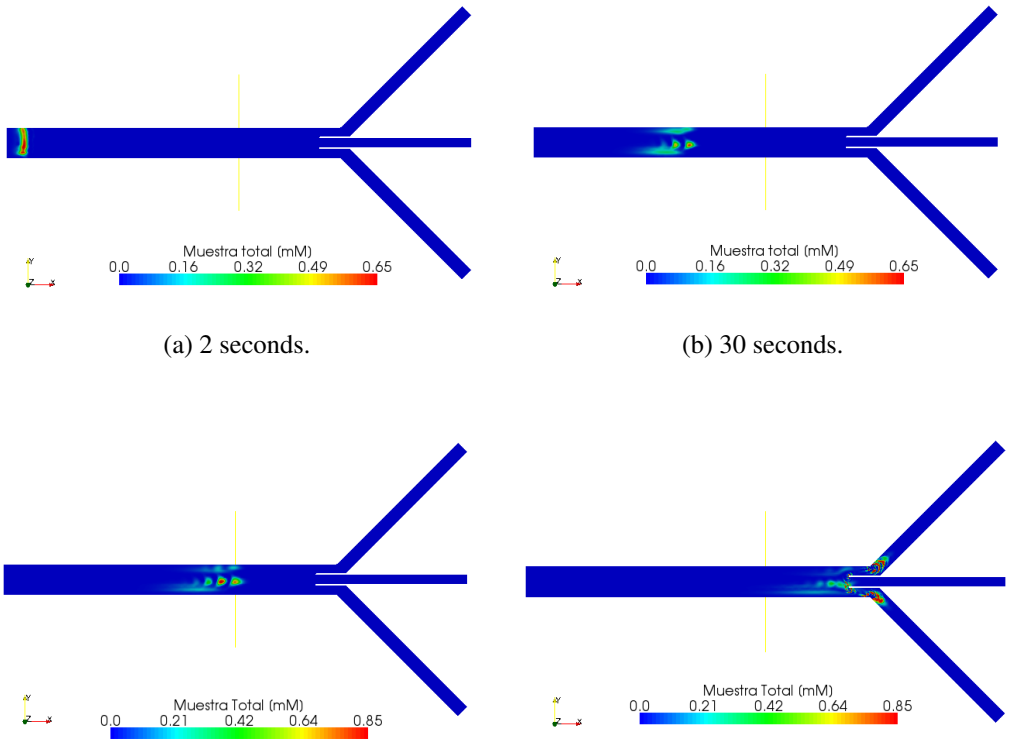

(a) 2 seconds. (b) 30 seconds.

(c) 50 seconds. (d) 70 seconds.

Figure 14: Total sample concentrations for t=2, 30, 50 and 70 seconds.

Component	pK_1	pK_2	pI	**Mobility** ($m^2V^{-1}s^{-1}$)
Protein 1	6.25	6.65	6.45	$3.0\ 10^{-8}$
Protein 2	6.47	6.87	6.67	$2.0\ 10^{-8}$
Protein 3	6.94	7.34	7.14	$3.0\ 10^{-8}$
Protein 4	7.17	7.57	7.37	$3.0\ 10^{-8}$
Protein 5	7.64	8.04	7.84	$2.0\ 10^{-8}$
Protein 6	7.87	8.27	8.07	$3.0\ 10^{-8}$

Table 3: Physicochemical properties for analyte constituents (proteins).

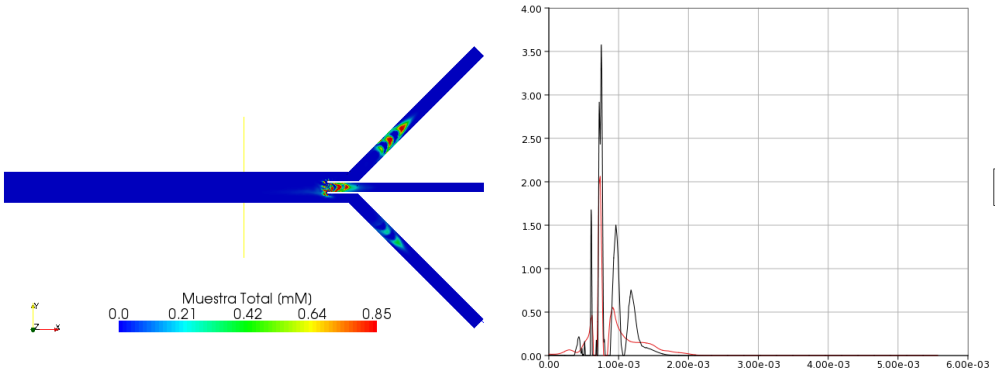

(a) Total sample distributions. (b) Center secondary channel.

Figure 15: Total sample distribution for t=90 seconds and equivalent electropherogram for the proteins 3 and 4 at central secondary channels.

5 CONCLUSIONS

The generalized numerical model for electrophoretic process discussed here results suitable for simulation of 1D and 2D electrophoretic separations in microfluidics chips. Strong coupling between equations that governs electrical phenomena, fluids dynamics, mass transport and chemical reactions was studied in example 4.1, which shows important practical consequences in focusing efficiency, or residence time. The model allows to simulate processes involving multiple analytes and complex electrolytes buffers as in example 4.2. Both example 4.1 and example 4.2 were validated by using data reported in the literature. Finally, an example of interest involving 2D electrophoresis, FFIEF and CZE on a μ-TAS was solved in example 4.3. This example show that the considered computational approach seems to be a suitable way to solve medium to large scale problems arising in the modelling and design of electrophoretic separations in microfluidics. In future works, certain problems related to numerical noise may be reduced in tridimensional domains.

6 ACKNOWLEDGEMENTS

This work has received financial support from Consejo Nacional de Investigaciones Científicas y Técnicas (CONICET, Argentina), Universidad Nacional del Litoral (UNL, Argentina) and Agencia Nacional de Promoción Científica y Tecnológica (ANPCyT, Argentina). Authors made extensive use of freely distributed software as GNU/Linux OS, MPI, PETSc, GCC compilers, Octave, Open-DX, Python, Perl, VTK, among many others.

REFERENCES

Arnaud I., Josserand J., Rossier J., and Girault H. Finite element simulation of off-geltm buffering. *Electrophoresis*, 23:3253–3261, 2002.

Balay S., Buschelman K., Gropp W.D., Kaushik D., Knepley M.G., McInnes L.C., Smith B.F., and Zhang H. PETSc Web page. 2008. http://www.mcs.anl.gov/petsc.

Barz D. and Ehrhard P. Fully-coupled model for electrokinetic flow and transport in microchannels. *PAMM*, 5(1):535–536, 2005.

Berli C., Piaggio M., and Deiber J. Modeling the zeta potential of silica capillaries in relation to the background electrolyte composition. *Electrophoresis*, 24:1587–1595, 2003.

Bianchi F., Ferrigno R., and Girault H. Finite element simulation of an electroosmotic-driven flow division at a t-junction of microscale dimensions. *Analytical Chemistry*, 72(9):1987–1993, 2000.

Chatterjee A. Generalized numerical formulations for multi-physics microfluidics-type applications. *Journal of Micromechanics and Microengineering*, 13:758–767, 2003.

Dalcín L. PETSc for Python. 2005-2008. http://petsc4py.googlecode.com/.

Dalcín L., Paz R., and D'Elia M.S.J. MPI for Python: Performance improvements and MPI-2 extensions. *Journal of Parallel and Distributed Computing*, 68(5):655–662, 2008.

Erickson D. Towards numerical prototyping of labs-on-chip: modeling for integrated microfluidic devices. *Microfluidics and Nanofluidics*, 1(4):301–318, 2005.

Ermakov S., Jacobson S., and Ramsey J. Computer simulations of electrokinetic transport in microfabricated channel structures. *Analytical Chemistry*, 70(21):4494–4504, 1998.

Ermakov S., Jacobson S., and Ramsey J. Computer simulations of electrokinetic injection techniques in microfluidic devices. *Analytical Chemistry*, 72(15):3512–3517, 2000.

Hruska V., Jaros M., and Gas B. Simul 5 - free dynamic simulator of electrophoresis. *Electrophoresis*, 27:984–991, 2006.

Hunter R. *Foundations of Colloid Science*. Oxford University Press, second edition, 2001.

Kirby B.and Hasselbrink Jr E. Zeta potential of microfluidic substrates: 1. theory, experimental techniques, and effects on separations. *Electrophoresis*, 25:187–202, 2004.

Kler P., Guarnieri F., and Berli C. Numerical simulation of electrokinetic flow in microfluidic chips. *Mecanica Computacional*, 25(28):2573–2584, 2006.

Kler P., Guarnieri F., and Berli C. Generalized numerical model for the simulation electrophoretic methods in microfluidic chips. *Mecanica Computacional*, 27:3367–3380, 2008.

Kler P., Guarnieri F., and Dalcin L. Efficient numerical model for electrokinetic flow in microfluidics systems with complex geometries. *Mecanica Computacional*, 26(5):485–497, 2007.

Kler P.A., López E.J., Dalcín L.D., Guarnieri F.A., and Storti M.A. High performance simulations of electrokinetic flow and transport in microfluidic chips. *Computer Methods in Applied Mechanics and Engineering*, 198(30-32):2360 – 2367, 2009.

Koch M., Evans A., and Brunnschweiler A. *Microfluidic technology and applications*. Research Studies Press Philadelphia, 2000.

Kohlheyer D., Besselink G.A.J., Schlautmann S., and Schasfoort R.B.M. Free-flow zone electrophoresis and isoelectric focusing using a microfabricated glass device with ion permeable membranes. *Lab on a Chip*, 6:374 – 380, 2006.

Li D. *Electrokinetics in Microfluidics*. Elsevier Academic Press, 2004.

Manz A., Graber N., and Widmer H. Miniaturized total chemical analysis systems: A novel concept for chemical sensing. *Sens. Actuators B*, 1:244–248, 1990.

Palusinski O.and Graham A., Mosher R., and Bier M.and Saville D. Theory of electrophoretic separations. part ii: Construction of a numerical scheme and its applications. *AICHE Journal*, 32(2):215–223, 1986.

Patankar N. and Hu H. Numerical simulation of electroosmotic flow. *Analytical Chemistry*, 70(9):1870–1881, 1998.

Probstein R. *Physicochemical Hydrodynamics. An Introduction*. Wiley-Interscience, second edition, 2003.

Reyes D., Iossifidis D., Auroux P., and Manz A. Micro total analysis systems. 1. introduction, theory, and technology. *Analytical Chemistry*, 74(12):2623–2636, 2002.

Saville D. and Palusinski O. Theory of electrophoretic separations. part i: Formulation of a mathematical model. *AICHE Journal*, 32(2):207–214, 1986.

Shim J., Dutta P., and Ivory C. Modeling and simulation of ief in 2-d microgeometries. *Electrophoresis*, 28:572–586, 2007.

Sommer G. and Hatch A. Ief in microfluidic devices. *Electrophoresis*, 30:742–757, 2009.

Sonzogni V.E., Yommi A.M., Nigro N.M., and Storti M.A. A parallel finite element program on a Beowulf cluster. *Advances in Engineering Software*, 33(7–10):427–443, 2002.

Storti M.A. Aquiles cluster at CIMEC. 2005-2008. http://www.cimec.org.ar/aquiles.

Tezduyar T., Mittal S., Ray S., and Shih R. Incompressible flow computations with stabilized bilinear and linear equal order interpolation velocity pressure elements. *Computer Methods in Applied Mechanics and Engineering*, 95:221–242, 1992.

Tezduyar T. and Osawa Y. Finite element stabilization parameters computed from element matrices and vectors. *Computer Methods in Applied Mechanics and Engineering*, 190(3-4):411–430, 2000.

Thormann W., Caslavska J., and Mosher R. Modeling of electroosmotic and electrophoretic mobilization in capillary and microchip isoelectric focusing. *Journal of Chromatography A*, 1155(2):154 – 163, 2007.